Climate change in the Canary/Iberia upwelling region: the role of ocean stratification and wind

Rubén Vázquez, Iván M Parras-Berrocal, William Cabos, Dmitry Sein, Rafael Mañanes, Marina Bolado-Penagos, Alfredo Izquierdo

ENVIRONMENTAL RESEARCH
LETTERS

LETTER • OPEN ACCESS

Climate change in the Canary/Iberia upwelling region: the role of ocean stratification and wind

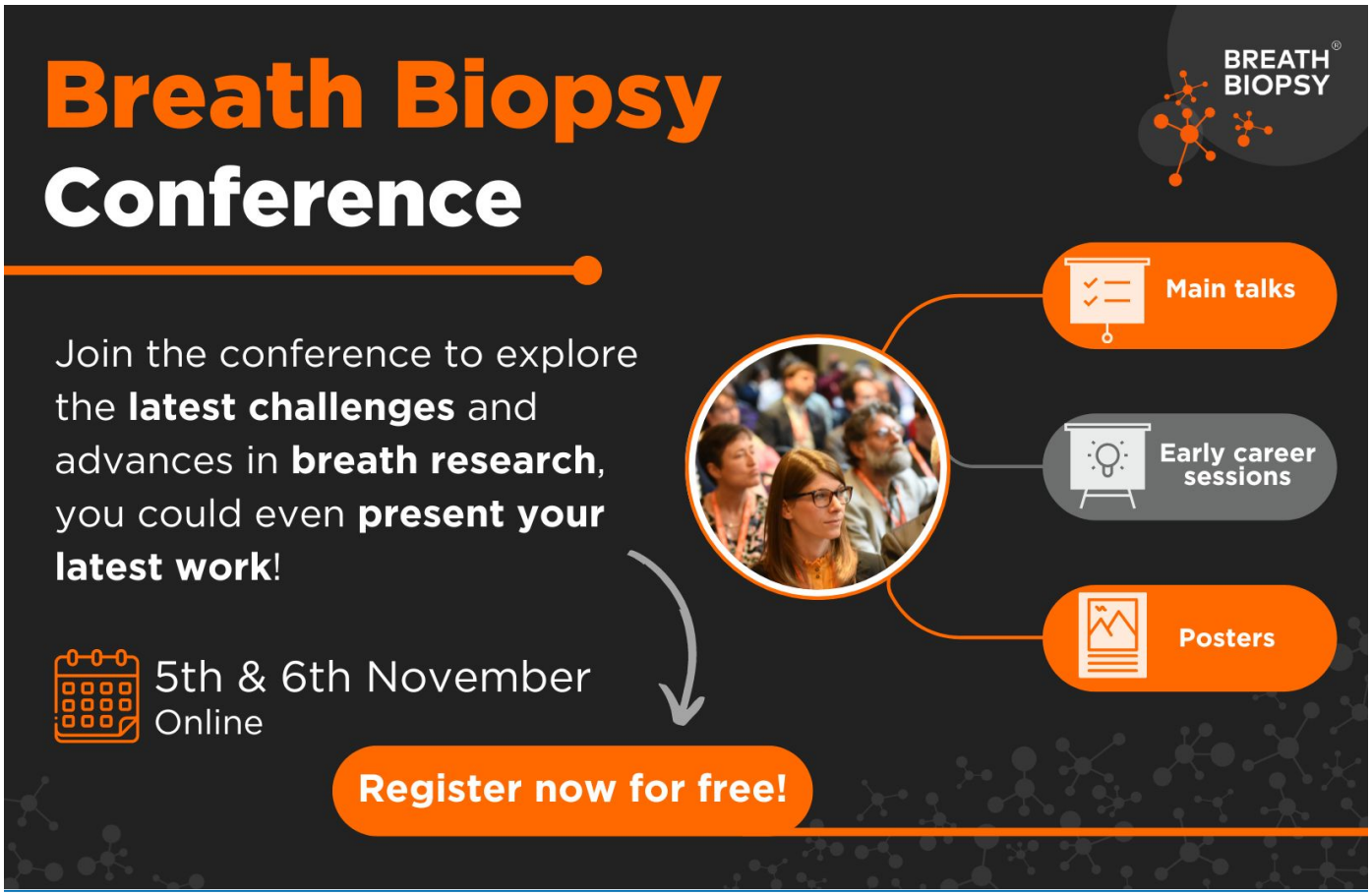

ENVIRONMENTAL RESEARCH
LETTERS

OPEN ACCESS

RECEIVED
1 March 2024

REVISED
13 June 2024

ACCEPTED FOR PUBLICATION
21 June 2024

PUBLISHED
8 July 2024

LETTER

Climate change in the Canary/Iberia upwelling region: the role of ocean stratification and wind

Rubén Vázquez[1], Iván M Parras-Berrocal[2], William Cabos[1], Dmitry Sein[3,4], Rafael Mañanes[5], Marina Bolado-Penagos[5] and Alfredo Izquierdo[5,*]

[1] Department of Physics and Mathematics, University of Alcalá, Alcalá de Henares 28801, Spain
[2] CNRM, Université de Toulouse, Météo-France, CNRS, Toulouse, France
[3] Alfred Wegener Institute for Polar and Marine Research, 27570 Bremerhaven, Germany
[4] Shirshov Institute of Oceanology, Russian Academy of Science, Moscow 117997, Russia
[5] Department of Applied Physics, Faculty of Marine and Environmental Sciences, Marine Research Institute (INMAR), University of Cádiz', Puerto Real, Cádiz 11510, Spain
* Author to whom any correspondence should be addressed.

E-mail: alfredo.izquierdo@uca.es

Keywords: coastal upwelling, climate change, ocean stratification, Azores High, upwelling index, Iberian thermal low, Canary/Iberia region

Supplementary material for this article is available online

Abstract

The Canary/Iberia region (CIR), part of the Canary Current Upwelling System, is well-known for its coastal productivity and crucial role in enriching the oligotrophic open ocean through the offshore transport of the upwelled coastal waters. Given its significant ecological and socio-economic importance, it is essential to assess the impact of climate change on this area. Therefore, the goal of this study is to analyze the climate change signal over the CIR using a high-resolution regional climate system model driven by the Earth system model MPI-ESM-LR under RCP8.5 scenario. This modelling system presents a regional atmosphere model coupled to a global ocean model with enough horizontal resolution at CIR to examine the role of the upwelling favourable winds and the ocean stratification as key factors in the future changes. CIR exhibits significant latitudinal and seasonal variability in response to climate change under RCP8.5 scenario, where ocean stratification and wind patterns will play both complementary and competitive roles. Ocean stratification will increase from the Strait of Gibraltar to Cape Juby by the end of the century, weakening the coastal upwelling all year long. This increase in stratification is associated with a freshening of the surface layers of the North Atlantic. However, modifications in the wind pattern will play a primary role in upwelling source water depth changes in the southernmost region of the CIR in winter and in the north of the Iberian Peninsula in summer. Wind pattern changes are related to the intensification of the Azores High in winter and to a deepening of the Iberian thermal low in summer months.

1. Introduction

The Canary Current Upwelling System (CCUS) is one of the four large Eastern Boundary Upwelling Systems (EBUSs) driven by equatorward alongshore winds. The upwelled cold and nutrient-rich waters do not only fuel the biological activity near the coast, but also behave as shelf and slope waters being transported to open ocean by active mesoscale structures (e.g. filaments, fronts, eddies [1–3]).

The CCUS extends from the coast of West Africa at 12° N to the northern tip of the Iberian Peninsula at 43° N and constitutes the eastern boundary of the North Atlantic subtropical gyre [4]. It is divided into four different regions: the Mauritania-Senegalese upwelling region (12° N–19° N), the permanent upwelling region (21° N–26° N; PUR) and the weak permanent upwelling region (26° N–33° N; WPUR) extending south and north of the Canary Islands, respectively, and the Iberian upwelling region (35° N–43° N; IUR), dominated by a high seasonal variability with upwelling favourable winds in summer and downwelling favourable winds during winter months [5–7].

Since the major mechanisms underpinning EBUSs originate from large-scale atmosphere-ocean coupling [8], the magnitude and timing of the EBUSs are sensitive and highly vulnerable to climate variability [9]. Several studies based on historical datasets analysis [6, 10–17] have striven to reveal the EBUSs response under climate change showing contradictory results, mainly due to the short duration of most observational time series [8] and methodological inconsistencies (e.g. considering only the upwelling season or annually averaged wind trends [15]).

A CMIP5 (Coupled Model Intercomparison Project) multi-model analysis of the upwelling response to climate change [18] found in the CCUS a robust relationship between the increase of the land–sea temperature contrast and the upwelling intensification in the twenty-first century (Bakun's hypothesis [19]). However, other studies suggested that the alongshore winds may be more sensitive to the intensity and position of the Azores High rather than to changes in the continental thermal low-pressure systems [20, 21]. In addition to wind changes, there are reports of warming of the upper ocean layer over the last decades, which leads to increased vertical stratification and reduced upward transport of nutrient-rich water to the surface [8, 22]. Thus, an increase in ocean stratification due to global warming would play a key role where deeper water might be less connected with the wind stress, shallowing the upwelling source water depth [23, 24] and becoming the main driver of changes in EBUSs during the 21st century (e.g. [23] in the Humboldt Upwelling System). As for CCUS, its future behaviour is still uncertain and both stratification and wind changes may play a complementary or competitive role [25].

However, the coarse spatial resolution (around $1^\circ \times 1^\circ$) of CMIP (both CMIP5 and CMIP6) models is not enough to resolve the latitudinal variability and to reproduce the mesoscale features or the shelf dynamics of the upwelling systems with enough detail [8, 26, 27]. Regional climate system models are able to account for mesoscale processes, which are not resolved by the global climate models [28, 29]. This ability to reproduce the mesoscale processes allows to assess the impact of climate change on CCUS in a more realistic way, given the importance of the eddies and coastal filaments that enrich the oligotrophic open waters [30–32].

The main objective of this work is to study the potential future impact of climate change over three northern regions (Canary/Iberia region; CIR) of the CCUS (figure 1) with a high resolution regional climate system model (the Mauritania–Senegalese upwelling region has been evaluated in a previous work [33]). For this purpose, this study aims to: (i) understand the impact of climate change on the wind field, identifying the main driver of future changes in the alongshore winds, and (ii) assess the impact of changes in ocean stratification due to global warming on coastal upwelling.

2. Material and methods

2.1. ROM configuration

We use the regional coupled system model ROM [34], composed of a global ocean model (MPIOM) coupled to an atmospheric regional model (REMO) via OASIS3 coupler [35]. ROM (REMO-OASIS-MPIOM) includes the lateral freshwater fluxes at the land surface through the Hydrological Discharge (HD) as part of REMO and the relevant carbon stocks of the atmosphere, ocean, and sediments through the Hamburg Ocean Carbon Cycle as a MPIOM subsystem [36, 37]. The ROM model has previously been evaluated over the CIR for the present climate in [29].

The oceanic component of ROM features a curvilinear grid with two poles, over North America and Northwestern Africa, yielding a grid size from 5 to 10 km in the CIR. This horizontal resolution is enough to reproduce some frontal mesoscale processes associated to the upwelling (i.e. eddies and filaments) while maintaining a global domain [29]. The model comprises 40 z-coordinate vertical levels with increasing level thickness towards the ocean bottom [33, 38]. REMO is integrated over a rotated regular grid with a horizontal resolution of 25 km and its domain includes the Eastern Tropical Pacific, the Mediterranean Sea and the North Atlantic (figure 1(b)), being the only model component of ROM run in regional configuration. In this work, ROM is driven by the low-resolution version ($1.5^\circ \times 1.5^\circ$) of the Max Planck Institute Earth System Model (MPI-ESM-LR) in two runs: first, a historical run from 1950 to 2005 and second, the climate projection from 2006 to 2099 under the Representative Concentration Pathway 8.5 (RCP8.5) CMIP5 scenario.

2.2. Upwelling analysis

To assess future changes in the seasonality and intensity of the coastal upwelling, we split the historical reference period (defined as 1976–2005; ROM_P1; 30 year climate normal) and the future climate (defined as 2070–2099; ROM_P2) into winter (December–January–February, DJF) and summer (June–July–August, JJA) seasons. These seasons correspond to upwelling peak (JJA) and minimum (DJF). Additionally, trends for the whole RCP8.5 simulation period (2006–2099) were calculated. We use monthly data of near-surface air temperature (T2m), mean sea level pressure (MSLP), wind stress, seawater temperature and salinity.

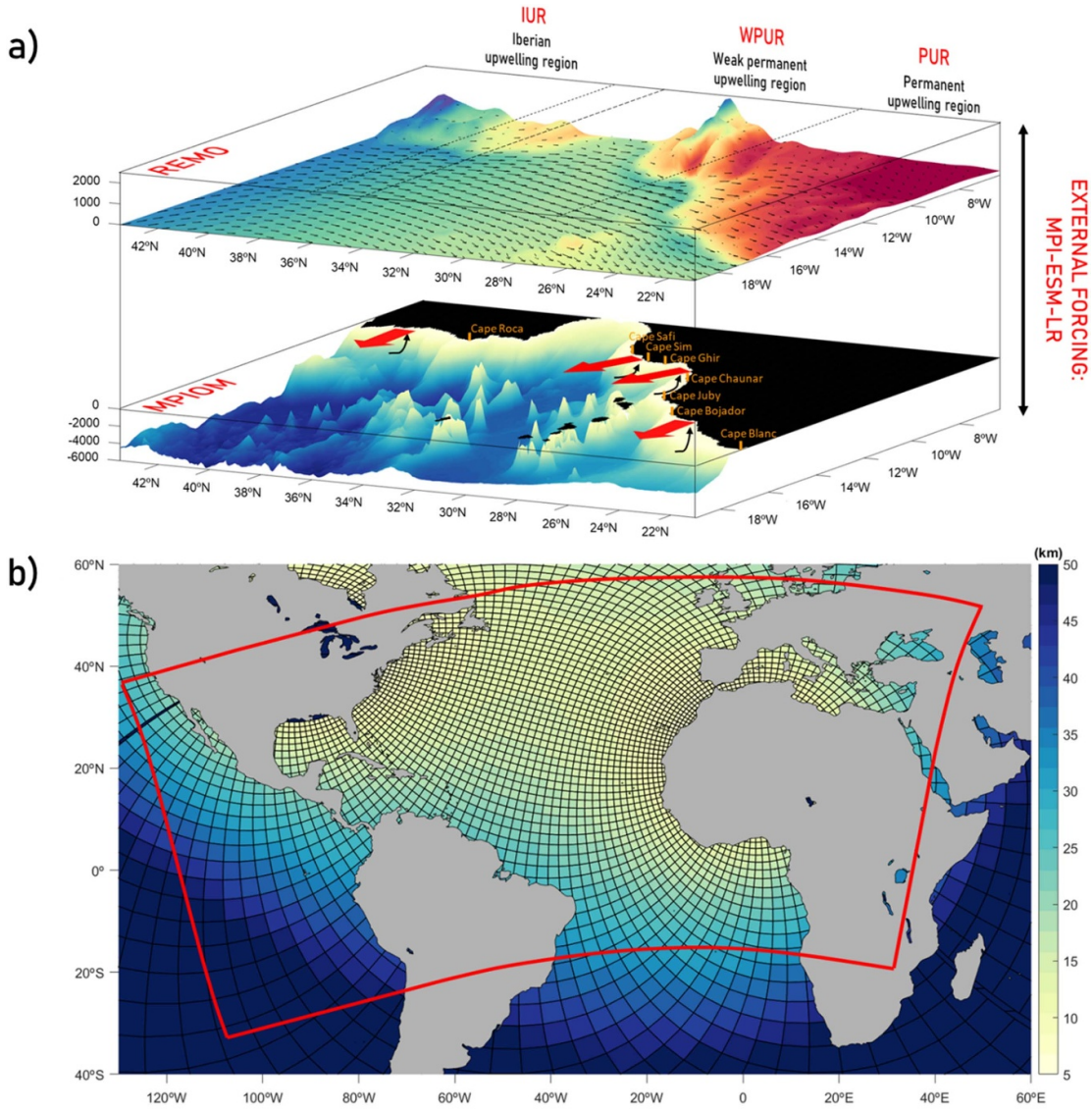

Figure 1. (a) Illustrative figure of ROM bathymetry (bottom), 2 m air temperature (T2m) and sea surface wind (top; vector field) fields for the ROM_P1 period in the three studied regions: Iberian upwelling region (IUR; 35° N–43° N), weak permanent upwelling region (WPUR; 26° N–33° N) and permanent upwelling region (PUR; 21° N–26° N). It shows the conceptual upwelling mechanism (thin black arrows) generated by the Ekman transport (red arrows). (b) MPIOM variable resolution bipolar curvilinear grid (black lines, drawn every 10th) and REMO domain (red line).

To quantify the upwelling intensity, we calculated the upwelling index (UI) derived from [39]:

$$Q_x = \frac{\tau_y}{f\rho_0} \tag{1}$$

$$Q_y = \frac{-\tau_x}{f\rho_0} \tag{2}$$

$$\mathrm{UI} = -\sin\left(\theta - \frac{\pi}{2}\right) Q_x + \cos\left(\theta - \frac{\pi}{2}\right) Q_y \tag{3}$$

where Q_x, Q_y and τ_x, τ_y are the zonal and meridional components of the horizontal Ekman transport ($m^2\ s^{-1}$) and the wind stress vector ($kg\ m^{-1}\ s^{-2}$), respectively; ρ_0 is the reference sea water density (1025 $kg\ m^{-3}$); f is the Coriolis parameter (s^{-1}) and θ is the angle between the coastline and the equator. Positive (negative) values of UI correspond to upwelling-favourable (downwelling-favourable) conditions.

However, the use of the UI overlooks the implication of the geostrophic flow in upwelling. Indeed, the cross-shore geostrophic transport can substantially alter the vertical transport relative to wind-based only estimates [40–43], and the inclusion of the geostrophic component is also important to understand how future changes in wind (e.g. [20]) will translate to changes in upwelling (e.g. [44]). Therefore, we define the Coastal Upwelling Transport Index (CUTI [45];) as the sum of UI and the cross-shore geostrophic transport (U^{geo}), an approach previously applied to coastal upwelling systems [42, 43, 45]. First, cross-shore geostrophic velocity (u^{geo}) is estimated from the alongshore sea surface height (SSH) gradient according to:

$$u^{geo} = \frac{g}{f}\frac{\Delta SSH}{d_{coast}} \quad (4)$$

where g is the gravitational acceleration, ΔSSH is the difference between the coastal SSH values at the northernmost and southernmost points in each cell, and d_{coast} is the distance (m) between these points. Second, the cross-shore geostrophic transport is calculated for the mixed layer:

$$U^{geo} = u^{geo}MLD \quad (5)$$

where mixed layer depth (MLD) is calculated using a density difference criterion (density increase by 0.125 kg m^{-3} compared to the value in the surface [46]) and taken from standard ROM outputs. In equation (5), it is assumed that cross-shore geostrophic velocity is constant throughout the MLD. Note that positive cross-shore geostrophic transport corresponds to offshore transport and negative to onshore transport.

Finally, we calculated the CUTI as the sum of UI and U^{geo}. The CUTI is estimated within a 100 km wide band along the CIR [29, 30] and it is expressed as the oceanward flow of surface waters per km of coastline (m^3 s^{-1} km^{-1}, [47]).

The coastal upwelling stratification is characterized through the Brunt-Väisälä frequency (N; s^{-1}), where larger values indicate strong stratification, and values close to zero a well-mixed water column:

$$N^2 = -\frac{g}{\rho_0}\frac{\partial \rho}{\partial z} \quad (6)$$

being z the depth and ρ the potential density.

Once the impact of the climate change on wind patterns and the ocean stratification is analyzed individually, we calculate the source water depth (Ds) to estimate the depth of the water that reaches the surface in the coastal upwelling region. Ds gives us further insight into the mechanisms that drive the coastal upwelling in the future, clarifying the role of the wind pattern and the coastal ocean stratification as complementary or competitive mechanisms. This parameter is defined in [48] as follows:

$$Ds = Cs\sqrt{\frac{CUTI}{N}} \quad (7)$$

where $Cs = (4/Ce)^{1/2} = 8.16$ for $Ce = 0.06$, which is the efficiency factor used in [48, 49]. Note that we have modified the equation for source water depth used in [48] to incorporate the influence of geostrophic transport on the source depth.

In this context, there are different methods to identify the source water depth with more accuracy, such as the use of Lagrangian particles (e.g. [44, 50, 51]) or the concentration of passive tracers (e.g. [52]) as source water markers. However, the temporal resolution of ROM model output (monthly) is too low to apply such approaches offline. Therefore, we resorted to this diagnostic to assess the source depth, which is simpler but allows a straightforward estimation of the relative contribution of wind and stratification changes to source water depth changes.

3. Results

3.1. Climate change signal of the coastal upwelling winds and its latitudinal variability

The significant seasonality of CIR poses a challenge in terms of assessing the impact of climate change. In this regard, we analyzed the CUTI in the historical simulation (ROM_P1) for DJF and JJA, as well as its trends for the RCP8.5 simulation (figure 2). In DJF, the CUTI shows negative values in the northern IUR due to downwelling favourable winds, while south of the IUR (from 37° N to 39° N) and south 34° N the CUTI turns positive, increasing as latitude decreases (figure 2(a)). It is noteworthy that both in Cape Roca (around 38° N) and north of WPUR (around the Strait of Gibraltar), the CUTI shows negative values, where precisely the onshore geostrophic transport seems to play an important role against the Ekman transport (figure 2(a)).

In DJF, CUTI trends exhibit large latitudinal variability, with negative values throughout the IUR, associated with an intensification of downwelling favourable winds northern IUR and a weakening of upwelling south of the IUR. The transitional region between the IUR and WPUR shows a marked shift from negative to positive trends. WPUR and PUR present positive trends, with the maximum located at Cape Bojador (figure 2(b)). Negative trends in the WPUR appear only at Cape Safi and Cape Ghir.

In JJA, the CUTI is positive throughout the CIR and increases with decreasing latitude peaking at Cape Sim and Cape Bojador (figure 2(c)). JJA CUTI trends show an almost opposite pattern to the DJF: IUR exhibits positive trends decreasing south, becoming negative from the Strait of Gibraltar to Cape Blanc (figure 2(d)). Also noteworthy are Cape Chaunar (located at nearly the same latitude as the Canary Islands, 29° N), Cape Bojador and Cape Blanc, where the negative trends locally weaken or even become positive (figure 2(d)). Contrary to the northern regions of the CIR in DJF, we find that the geostrophic flow is everywhere secondary compared to the wind-driven transport in JJA (figure 2(c)). The remarkable peaks observed in the CUTI are primarily associated with coastline or topo-bathymetric irregularities, which impact on the wind field and generate mesoscale structures such as filaments and fronts [53]. One of the advantages of the model utilized in the present study is its capability to capture these processes [29].

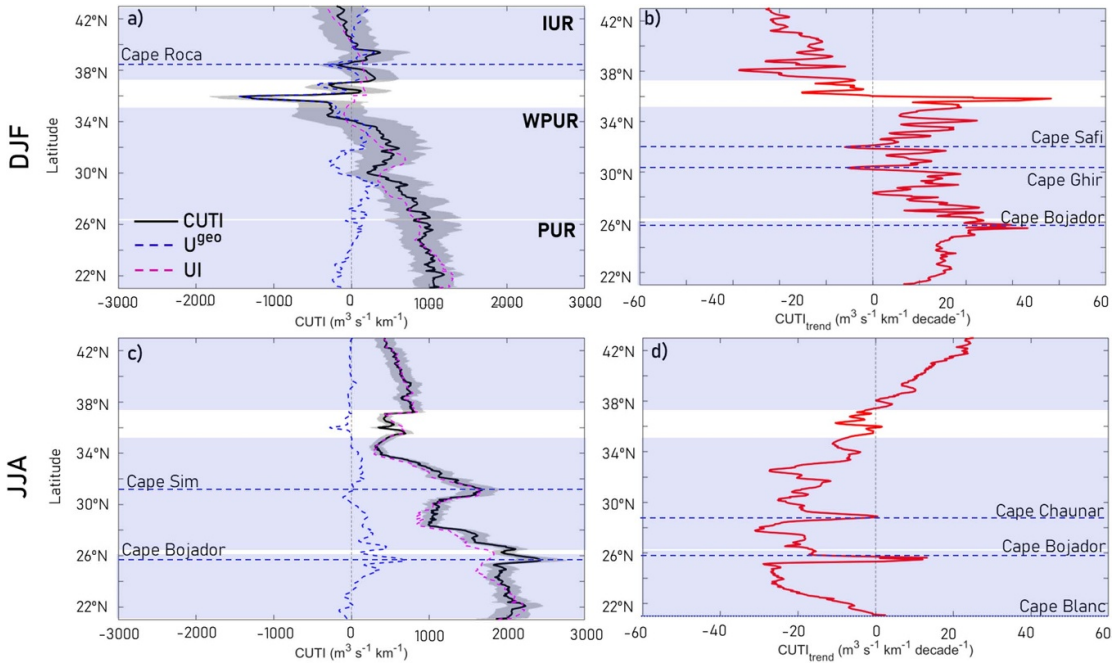

Figure 2. *CUTI*, U^{geo} and UI (m^3 s^{-1} km^{-1}) in the closest grid points to coast for ROM_P1 (1976–2005) in DJF (a) and JJA (c) and its standard deviation (grey shaded). CUTI trend (m^3 s^{-1} km^{-1} decade^{-1}) from 2006 to 2099 for DJF (b) and JJA (d).

3.2. Climate change drivers of the coastal upwelling winds

As shown in section 3.1, changes in CUTI are clearly seasonal, so it is reasonable to assess the potential drivers of these changes on a seasonal basis. To this end, we evaluated the future evolution of both MSLP and T2m on a seasonal basis.

In DJF, ROM_P1 presents the highest T2m over the ocean in the southern regions (around 20° N; figure 3(a)), but the largest temperature increase at the end of the century is localized over the African continent, reaching trends of 0.16 °C decade^{-1} in the Atlas Mountains (figure 3(b)). There are also moderate warming trends over the Iberian Peninsula and some ocean regions.

MSLP in the historical period features the Azores High centered between 30° and 35° N. Notably, the Azores High shows an increase in both extent and intensity in ROM_P2 (dashed isobars in figure 3(c)), corresponding to a general MSLP increase across the domain, more pronounced over the ocean. Wind differences between ROM_P2 and ROM_P1 are shown alongside trends, displaying northward directions in the IUR and southward from around 30° N to Cape Blanc, i.e. downwelling favourable winds in IUR and upwelling favourable winds over most of WPUR and PUR. Thus, the intensification of the Azores High in DJF will increase downwelling and upwelling favourable winds in the IUR and PUR, respectively (figure 2(b)).

JJA T2m values are logically higher than in DJF, with very warm temperatures over Africa (figure 4(a)). JJA T2m trends are very strong over Africa and the Iberian Peninsula, with values exceeding 0.20 °C decade^{-1} (figure 4(b)) but coastal regions show slightly weaker increases. In the MSLP field, the Azores High migrates northwestward respect to DJF, and its position and extent are rather similar in ROM_P1 and ROM_P2 (see isobaric contours in figure 4(c)). The summer thermal low over the Iberian Peninsula intensifies in ROM_P2 due to the local T2m increase. Additionally, there is a MSLP increase over the British Isles that decreases the meridional MSLP gradient. As a result the wind field corresponding to the ROM_P2—ROM_P1 MSLP difference depicts a cyclonic rotation over the Iberian Peninsula, causing an increase in upwelling favourable winds in the IUR (figure 4(f)), and SW winds along most of the African coast, weakening the upwelling favourable winds (figure 4(f)). The spatial pattern of the MSLP difference between ROM_P2 and ROM_P1 causing these wind changes is shown in figure S2. Therefore, in JJA, the intensification of the Iberian thermal low generates an increase of the Iberian upwelling (figure 2(d)).

3.3. Ocean stratification

In this section, we study the role of the ocean stratification as a driver of change in the CIR regions. Ocean stratification changes in the CIR for DJF and JJA are evaluated from the Brunt-Väisälä frequency calculated within a 100 km wide band along the CIR (the mask is shown in figure 5(c)) and averaged from surface to 150 m depth (approximate depth at which water masses upwell in the CIR [29]).

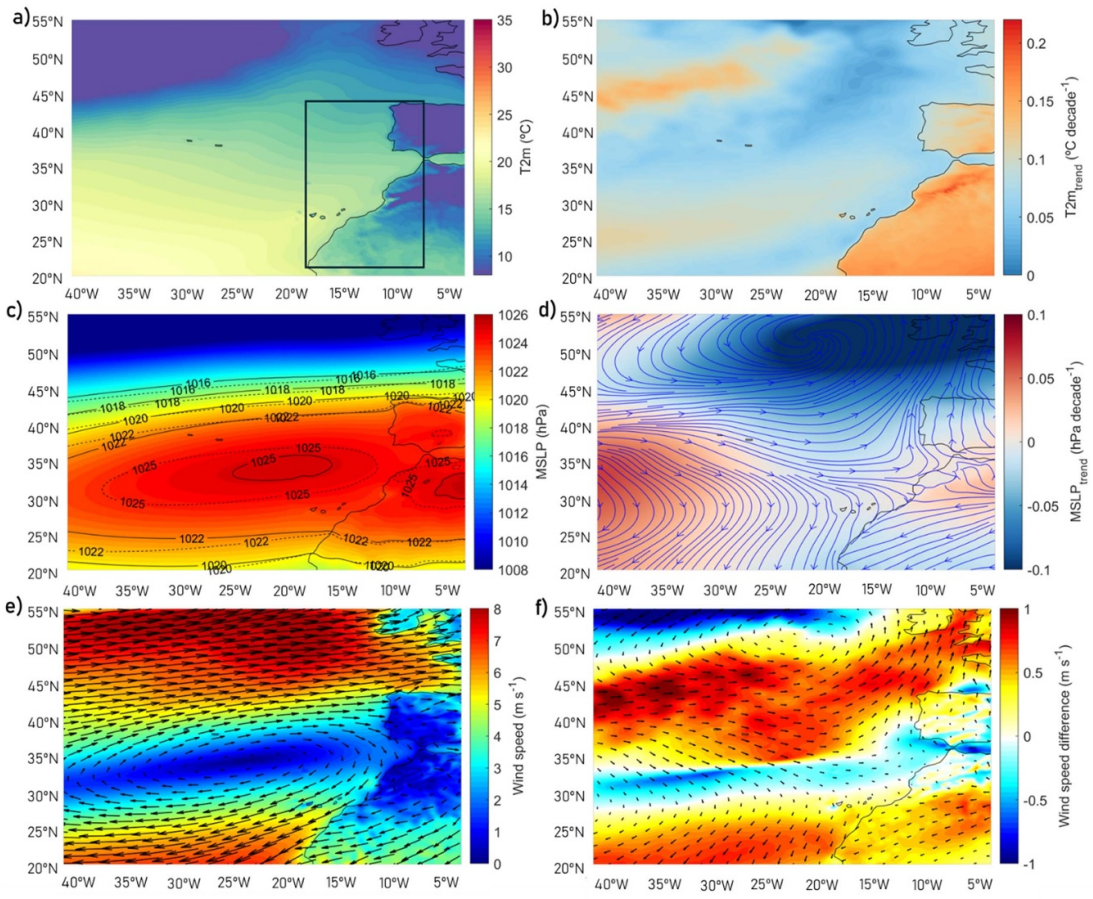

Figure 3. (a) Mean T2m (°C) for ROM_P1 (1976–2005) and (b) T2m trend (°C decade^{-1}) from 2006 to 2099 in DJF. (c) Mean MSLP (hPa) for ROM_P1 (1976–2005) and (d) MSLP trend (hPa decade^{-1}) from 2006 to 2099 in DJF. In (c) the isobars are presented for both ROM_P1 (continuous black line) and ROM_P2 (dashed black line) simulations. In (d) Wind flowlines (blue) corresponding to the ROM_P2 -ROM_P1 difference, which are superimposed on the ROM_P2 MSLP trend. (e) Mean wind speed (m s^{-1}) for ROM_P1 (1976–2005) and (f) wind speed difference between ROM_P2 and ROM_P1.

In ROM_P1 DFJ the Brunt-Väisälä frequency is below 0.005 s^{-1} throughout the CCUS (excluding PUR). In this regard, the values remain relatively constant from the northernmost Iberian Peninsula to 25° N, where they progressively increase up to 0.008 s^{-1} at Cape Blanc (figure 5(a)). In JJA, stratification increases due to surface warming and shows larger latitudinal variability than DJF, with peaks at the Strait of Gibraltar, Cape Juby and Cape Blanc (figure 5(b)).

To assess ocean stratification changes in the future, we calculated the differences between ROM_P2 and ROM_P1 (grey shading). In DJF, the Brunt-Väisälä frequency increases up to 0.003 s^{-1} throughout the IUR and WPUR, nearly doubling the ROM_P1 values (figure 5(a)). South of 26° N the differences decrease drastically, even reaching negative values in the PUR. In JJA, the increase in stratification by the end of the century is also evident, but the relative change with respect to the historical period is smaller than in DJF (figure 5(b)). Nevertheless, the increase shows peaks reaching 0.003 s^{-1} in some regions of the African coast. As in DJF, the differences gradually decrease south of 26° N.

3.4. Source water depth

With the aim of linking the changes associated with the wind field and the ocean stratification, in this section we analyse the upwelling source depth taking into consideration both the action of the alongshore favourable winds and the ocean stratification (see equation (7)).

The source depth of the upwelling increases as latitude decreases in ROM_P1 for both DJF and JJA (figures 6(a) and (c)). The main differences between seasons are found in the IUR, where in DJF there is no upwelling in the north and a disruption in upwelling at Cape Roca and to the south of the Iberian Peninsula (Strait of Gibraltar). Regarding the African coast, slightly deeper source water is observed in JJA, with maxima at Cape Ghir and Cape Bojador.

Under RCP8.5 scenario a shallowing is expected for DJF in the IUR (40 m) and in the WPUR (20 m), and a deepening in the southernmost region, PUR

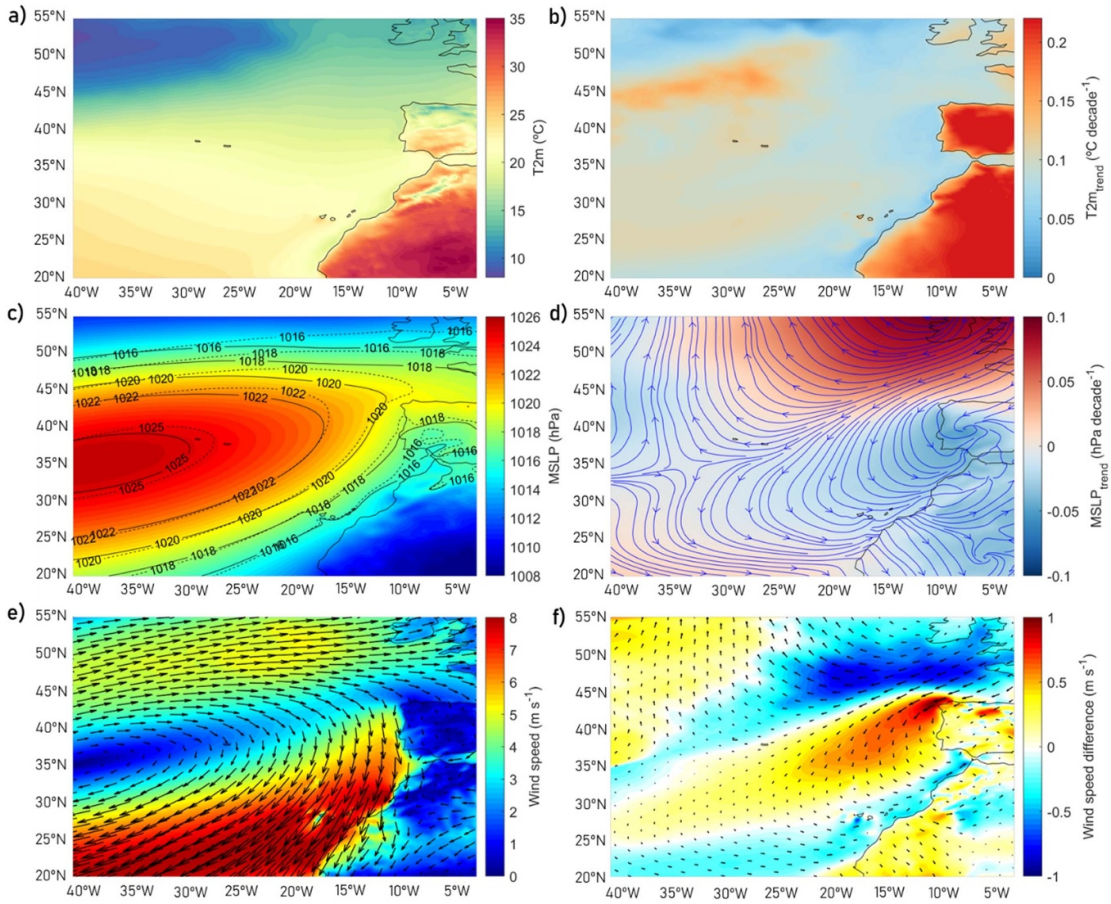

Figure 4. Same as figure 3, but for JJA.

(10 m; figure 6(b)). In JJA, we find a rather different pattern, where the northern part of the IUR shows an increase in source water depth, which decreases south of the IUR until practically Cape Blanc. It is noteworthy that this decrease in source depth is softened in PUR.

4. Discussion and conclusions

Future climate change has important biological and socio-economic implications in the upwelling regions [27] associated with changes in the upwelling favourable winds and increasing ocean stratification [8]. Here, we take advantage of the regional climate system model ROM to attain oceanic and atmospheric resolutions that allow us to study the climate change in the CIR while taking into account the impact of the mesoscale [29, 33]. Our assessment is based on the RCP8.5 CMIP5 scenario, using the ROM model driven by the MPI-ESM-LR. Our single model approach imposes limitations on the generalization of our results, however it makes it easier to analyse and find physically consistent mechanisms responsible for these changes, providing a foundation for future exploration with other models and forcings. Furthermore, one of the strengths of our study is associated with the high resolution presented by ROM, never before seen in the study of climate change at the CIR.

This work brings the novelty of advancing in one of the main scientific uncertainties within the EBUSs community regarding the roles of wind and oceanic stratification. Additionally, it unveils different climate change mechanisms and responses at CIR depending on latitude and seasonality. While the IUR exhibits a strengthening of downwelling favourable winds in DJF and upwelling favourable winds in JJA in its northern region (e.g. [21, 54, 55]), along the African coast it is projected a decrease in the upwelling favourable winds in the JJA and an increase in DJF. Similar results were obtained with the AFRICA-CORDEX ensemble model [56], confirming the seasonal signal of the upwelling change in the CIR under global warming conditions found in this study. Furthermore, the Ekman suction presents trends of the same sign, but weaker than the Ekman transport along the CIR (figure S1). In our assessment of the coastal upwelling we take into consideration the contribution of the geostrophic transport. In this context, we find that although the geostrophic transport

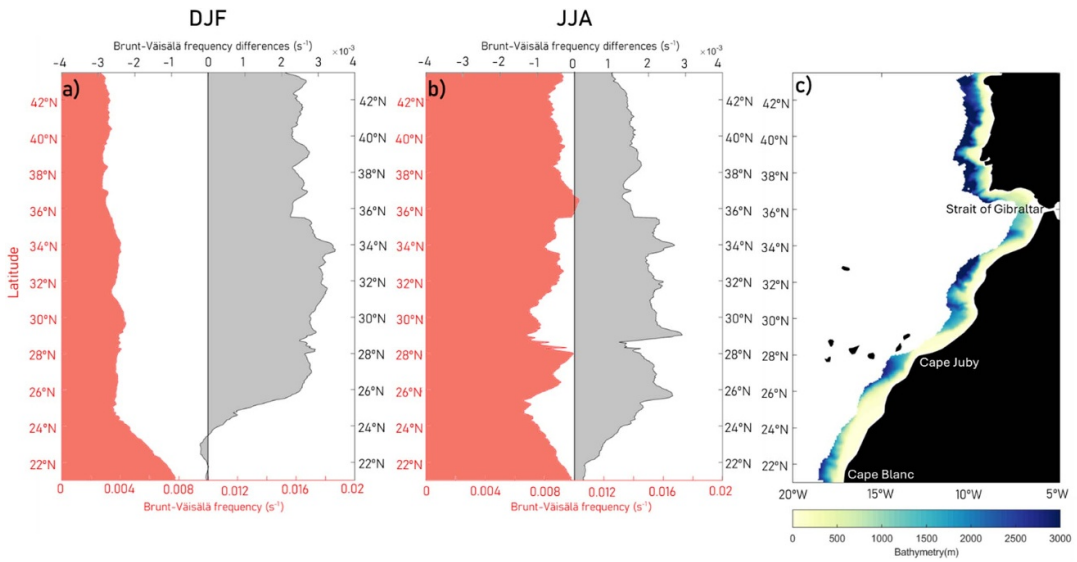

Figure 5. Brunt-Väisälä frequency (s^{-1}) averaged from surface to 150 m in the closest grid points to coast for DJF (a) and JJA (b) for ROM_P1 (red shading) and the differences between ROM_P2 and ROM_P1 (grey shading; RCP8.5—Historical). The mask used is shown in the panel (c).

makes a contribution to the cross-shore transport in JJA, it is of secondary importance compared to the Ekman transport (figure 2(c)). These results are consistent with those of [57], which showed that the onshore geostrophic transport was much lower than the offshore transport generated by upwelling favourable winds, especially in the MPI-ESM model (ROM driving model). However, during DJF in some regions of IUR and WPUR the geostrophic transport makes a contribution comparable to that of the wind (figure 2(a)). Finally, our results also project a future reduction in CUTI interannual variability in the IUR and WPUR during DJF (not shown).

Our results demonstrate that the impact of climate change on the wind field exhibits significant latitudinal and seasonal variability in the CIR. This variability is primarily associated with two mechanisms, one for each studied season (1) in DJF, the intensification of the Azores High will increase downwelling and upwelling favourable winds in the IUR and PUR, respectively; (2) in JJA, the intensification of the Iberian thermal low generates an increase of the Iberian upwelling. Previous studies have found changes in the wind pattern similar to those shown in this work [8, 18, 20, 21, 27, 56, 58, 59]. However, all of them addressed the effect of climate change through a single mechanism, either associated with increasing summertime T2m land-sea differences [19] or shifts in the positioning of the atmospheric high-pressure systems [20]. Our study reveals that the Azores High will play a fundamental role in the future of the CIR for DJF as proposed by other authors. However, we find a different mechanism of change for the summer season: the Iberian thermal low will deepen in the future due to the strong air temperature increase over the Iberian Peninsula in JJA, intensifying the Iberian upwelling (figure 4 [60, 61]).

Our results reveal an increase in ocean stratification in coastal regions, particularly evident in the two northernmost regions during both DJF and JJA (figure 5). This is attributable to the surface ocean warming. However, in the future, it is also projected a freshening in the upper 200 m of CIR, leading to an additional enhancement of stratification in shallow regions close to the shelf. This pattern is linked to a larger-scale freshening signal in the Eastern North Atlantic (figure S3) and consistent with findings reported by [62] in a study using CMIP5 models. The Canary Current transports the freshening signal to the south along the CIR, separating from the coast at Cape Blanc where it merges with the North Equatorial Current [63–65], therefore the PUR remains relatively unaffected by the freshening.

The upwelling source water depth will be reduced in the southern region of the IUR and throughout the WPUR for DJF. This shallowing in winter months is primarily associated with changes in ocean stratification in WPUR and with both, changes in ocean stratification and wind, in IUR (figure S4(a)). These results are consistent with studies such as [23] in the Humboldt Upwelling System and [24] in the north of the Iberian Peninsula. However, in JJA in the north of the Iberian Peninsula, the upwelling source depth will increase as consequence of the

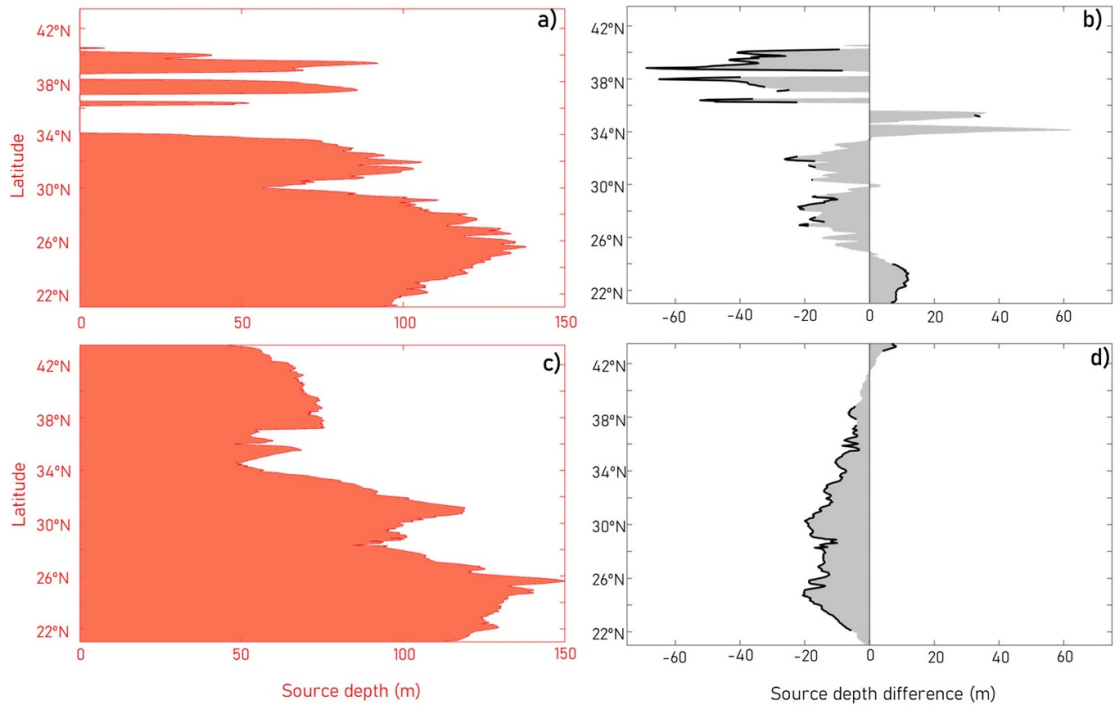

Figure 6. Upwelling source water depth (m) in the closest grid points to coast DJF (a) and JJA (c) both for ROM_P1 (red shading; Historical) and the differences between ROM_P2 and ROM_P1 (grey shading; RCP8.5—Historical), for DJF (b) and JJA (d). The mask used for source water depth calculation is shown in figure 5(c). Note that the black contour lines marked on panels b and d indicate statistically significant changes (t-student test).

future intensification of the upwelling favourable winds (figure S4(b)). Other recent studies report a future source water deepening in the CIR [66] and in the Mauritanian-Senegalese upwelling region [33]. However, in the rest of the CCUS regions, enhanced ocean stratification complements weakening upwelling winds, causing a shallower upwelling. This demonstrates that while using averaged variables for studying different EBUSs provides useful information, the significant latitudinal and seasonal variability in these systems could obscure the signal of climate change. It should be noted that the calculation of the presented source depth only takes into account the effect of stratification and the Ekman and geostrophic transports, although topography can play an important role in shaping upwelling structure [67–69], and therefore on source water depth.

Finally, to clarify the signal of climate change in the studied regions of the CCUS, a scheme of the interplay between wind and oceanic stratification was plotted (figure 7). Note that when referring to complementarity, we consider simultaneously an increase (decrease) in upwelling favourable winds along with a decrease (increase) in ocean stratification. When referring to competition, we consider simultaneously an increase (decrease) in upwelling favourable winds along with an increase (decrease) in ocean stratification.

In this context, it is observed that during DJF (figure 7), both mechanisms are complimentary (64% upwelling winds and 36% ocean stratification) leading to a shoaling of the source depth by 25 m south of the IUR. This complementarity turns into competition from the Strait of Gibraltar to 25° N, where increased stratification (57%) results in a 10 m shoaling of the source depth despite increasing upwelling favourable winds. In JJA, wind and oceanic stratification compete with different outcomes in the IUR; to the north, it deepens (by 5 m) due to the wind action (67%), and to the south, it shoals (by 5 m) due to stratification (67%). Once again, along the African coast, both mechanisms complement each other, leading to a shoaling of around 15 m. These results highlight the need to conduct studies on the seasonal and latitudinal variability of upwelling systems, as demonstrated here by the challenges of pinpointing a dominant mechanism for the upwelling response to climate change by the end of the century.

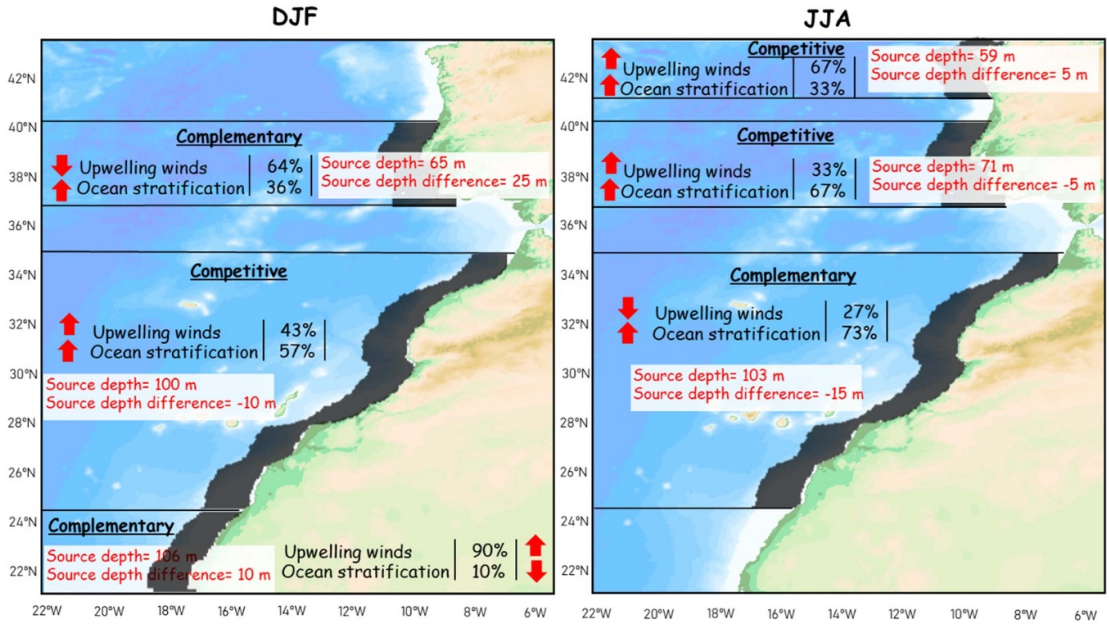

Figure 7. Scheme of complementarity and competitivity between ocean stratification and wind in the study regions. We consider only regions where future changes in water source depth are larger than 5 m (black shaded areas). Note that the wind contribution is calculated based on the CUTI (i.e. including the geostrophic transport). Additionally, the percentages correspond to the contribution of wind and ocean stratification to changes in source depth. When both are complementary, the result of the source depth differences shows contributions from both. However, when they compete, the higher percentage indicates dominance in the sign of the source depth change. Source depth change is calculated from an average of ROM_P2 minus ROM_P1 in each region.

Data availability statement

The data that support the findings of this study are openly available at the following URL/DOI: https://doi.org/10.5281/zenodo.10696742.

Acknowledgments

R Vázquez and W Cabos were supported by the Spanish Ministry of Science, Innovation and Universities, Through Grants (I+D+I PID2021-128656OB-I00). Dmitry Sein was supported by the Germany-Sino Joint Project (ACE, Nos. 2019YFE0125000 and 01LP2004A) and the scientific task N° FMWE-2024-0028 of MHESRF. M Bolado-Penagos was supported by Plan Propio Investigadores Noveles UCA (BOLA—PR2023-030) and the CEIMAR Jóvenes Investigadores (ASTRAL—CEI-JD-23-08).

ORCID iDs

Rubén Vázquez https://orcid.org/0000-0002-8910-5583
Iván M Parras-Berrocal https://orcid.org/0000-0003-4659-3924
William Cabos https://orcid.org/0000-0003-3638-6438
Dmitry Sein https://orcid.org/0000-0002-1190-3622
Rafael Mañanes https://orcid.org/0000-0003-1987-478X
Marina Bolado-Penagos https://orcid.org/0000-0002-6036-5840
Alfredo Izquierdo https://orcid.org/0000-0003-3842-1460

References

[1] Pelegrí J L, Aristegui J, Cana L, González-Dávila M, Hernández-Guerra A, Hernández-León S, Marrero-Díaz A, Montero M F, Sangrá P and Santana-Casiano M 2005 Coupling between the open ocean and the coastal upwelling region off northwest Africa: water recirculation and offshore pumping of organic matter *J. Mar. Syst.* **54** 3–37
[2] Álvarez-Salgado X A, Arístegui J, Barton E D and Hansell D A 2007 Contribution of upwelling filaments to offshore carbon export in the subtropical Northeast Atlantic Ocean *Limnol. Oceanogr.* **52** 1287–92
[3] Sangrá P 2015 Canary Islands eddies and coastal upwelling filaments off North-west Africa *Oceanographic and Biological Features in the Canary Current Large Marine Ecosystem* ed L Valdés and I Déniz-González (IOC-UNESCO, IOC Technical Series) pp 105–14
[4] Pelegrí J L and Peña-Izquierdo J 2015b Eastern boudary currents off Northwest Africa *Oeanographic and Biological Features in the Canary Current Large Marine Ecosystem* ed L Váldes and I Déniz-González (IOC-UNESCO, Technical Series 115) ch 3.3, pp 115–383
[5] Arístegui J, Barton E D, Álvarez-Salgado X A, Santos A M P, Figueiras F G, Kifani S, Hernández-León S, Mason E, Machú E and Demarcq H 2009 Sub-regional ecosystem variability in the Canary Current upwelling *Prog. Oceanogr.* **83** 33–48

[6] Cropper T E, Hanna E and Bigg G R 2014 Spatial and temporal seasonal trends in coastal upwelling off Northwest Africa, 1981–2012 *Deep Sea Res.* **86** 94–111
[7] Gómez-Letona M, Ramos A G, Coca J and Arístegui J 2017 Trends in primary production in the Canary Current Upwelling System a regional perspective comparing remote sensing models *Front. Mar. Sci.* **4** 370
[8] García-Reyes M, Sydeman W J, Schoeman D S, Rykaczewski R R, Black B A, Smit A J and Bograd S J 2015 Under pressure: climate change, upwelling, and eastern boundary upwelling ecosystems *Front. Mar. Sci.* **2** 109
[9] Macias D, Landry M R, Gershunov A, Miller A J and Franks P J S 2012 Climatic control of upwelling variability along the western North American coast *PLoS One* **7** e30436
[10] Bakun A, Field D B, Redondo-Rodriguez A N A and Weeks S J 2010 Greenhouse gas, upwelling-favorable winds, and the future of coastal ocean upwelling ecosystems *Glob. Change Biol.* **16** 1213–28
[11] Narayan N, Paul A, Mulitza S and Schulz M 2010 Trends in coastal upwelling intensity during the late 20th century *Ocean Sci.* **6** 815–23
[12] Gutiérrez D *et al* 2011 Coastal cooling and increased productivity in the main upwelling zone off Peru since the mid-twentieth century *Geophys. Res. Lett.* **38** 1–6
[13] Santos F, DeCastro M, Gómez-Gesteira M and Álvarez I 2012 Differences in coastal and oceanic SST warming rates along the Canary upwelling ecosystem from 1982 to 2010 *Cont. Shelf Res.* **47** 1–6
[14] Barton E D, Field D B and Roy C 2013 Canary Current Upwelling: more or less? *Prog. Oceanogr.* **116** 167–78
[15] Sydeman W J, Garcia-Reyes M, Schoeman D S, Rykaczewski R R, Thompson S A, Black B A and Bograd S J 2014 Climate change and wind intensification in coastal upwelling ecosystems *Science* **345** 77–80
[16] Bakun A, Black B A, Bograd S J, Garcia-Reyes M, Miller A J, Rykaczewski R R and Sydeman W J 2015 Anticipated effects of climate change on coastal upwelling ecosystems *Curr. Clim. Change Rep.* **1** 85–93
[17] Varela R, Alvarez I, Santos F, deCastro M and Gomez-Gesteira M 2015 Has upwelling strengthened along worldwide coasts over 1982–2010? *Sci. Rep.* **5** 10016
[18] Wang D W, Gouhier T C, Menge B A and Ganguly A R 2015 Intensification and spatial homogenization of coastal upwelling under climate change *Nature* **518** 390–4
[19] Bakun A 1990 Global climate change and intensification of coastal ocean upwelling *Science* **247** 198–201
[20] Rykaczewski R R, Dunne J P, Sydeman W J, Garcia-Reyes M, Black B A and Bograd S J 2015 Poleward displacement of coastal upwelling-favorable winds in the ocean's eastern boundary currents through the 21st century *Geophys. Res. Lett.* **42** 6424–31
[21] Sousa M C, de Castro M, Álvarez I, Gomez-Gesteira M and Dias J M 2017a Why coastal upwelling is expected to increase along the Western Iberian Peninsula over the next century? *Sci. Total Environ.* **592** 243–51
[22] Di Lorenzo E, Miller A J, Schneider N and McWilliams J C 2005 The warming of the California current system: dynamics and ecosystem implications *J. Phys. Oceanogr.* **35** 336–62
[23] Oyarzún D and Brierley C M 2019 The future of coastal upwelling in the Humboldt current from model projections *Clim. Dyn.* **52** 599–615
[24] Sousa M C, Ribeiro A, Des M, Gomez-Gesteira M, deCastro M and Dias J M 2020 NW Iberian Peninsula coastal upwelling future weakening: competition between wind intensification and surface heating *Sci. Total Environ.* **703** 134808
[25] Bonino G, Di Lorenzo E, Masina S and Iovino D 2019 Interannual to decadal variability within and across the major Eastern boundary upwelling systems *Sci. Rep.* **9** 1–14
[26] Xiu P, Chai F, Curchitser E and Castruccio F 2018 Future changes in coastal upwelling ecosystems with global warming: the case of the California current system *Sci. Rep.* **8** 2866
[27] Varela R, Rodríguez-Díaz L, de Castro M and Gómez-Gesteira M 2022 Influence of Canary upwelling system on coastal SST warming along the 21st century using CMIP6 GCMs *Glob. Planet. Change* **208** 103692
[28] Bindoff N L *et al* 2019 Changing ocean, marine ecosystems, and dependent communities *IPCC Special Report on the Ocean and Cryosphere in a Changing Climate* ed H-O Pörtner *et al* (Cambridge University Press) pp 447–587
[29] Vázquez R, Parras-Berrocal I, Cabos W, Sein D V, Mañanes R and Izquierdo A 2022 Assessment of the Canary current upwelling system in a regionally coupled climate model *Clim. Dyn.* **58** 69–85
[30] Lovecchio E, Gruber N, Münnich M and Lachkar Z 2017 On the longrange offshore transport of organic carbon from the canary upwelling system to the open North Atlantic *Biogeosciences* **14** 3337–69
[31] Lovecchio E, Gruber N and Münnich M 2018 Mesoscale contribution to the long-range offshore transport of organic carbon from the canary upwelling system to the open North Atlantic *Biogeosciences* **15** 5061–91
[32] Hailegeorgis D, Lachkar Z, Rieper C and Gruber N 2021 A Lagrangian study of the contribution of the Canary coastal upwelling to the open North Atlantic nitrogen budget *Ocean Sciences Meeting* (AGU) (https://doi.org/10.5194/bg-18-303-2021)
[33] Vázquez R, Parras-Berrocal I M, Koseki S, Cabos W, Sein D V and Izquierdo A 2023 Seasonality of coastal upwelling trends in the mauritania-senegalese region under RCP8. 5 climate change scenario *Sci. Total Environ.* **898** 166391
[34] Sein D V, Mikolajewicz U, Gröger M, Fast I, Cabos W, Pinto J G, Hagemann S, Semmler T, Izquierdo A and Jacob D 2015 Regionally coupled atmosphere-ocean-sea ice-marine biogeochemistry model ROM: 1. Description and validation *J. Adv. Model Earth Syst.* **7** 268–304
[35] Valcke S 2013 The OASIS3 coupler: a European climate modelling community software *Geosci. Model Dev.* **6** 373–88
[36] Parras-Berrocal I, Vázquez R, Cabos W, Sein D, Mañanes R, Perez-Sanz J and Izquierdo A 2020 The climate change signal in the Mediterranean sea in a regionally coupled ocean-atmosphere model *Ocean Sci.* **16** 743–65
[37] Sein D V *et al* 2020 Regionally coupled atmosphere—ocean—marine biogeochemistry model ROM: 2. Studying the climate change signal in the North Atlantic and Europe *James* **12** e2019MS001646
[38] Soares P M, Lima D C, Semedo A, Cabos Narvaez W D and Sein D 2019 Climate change impact on the Northwestern African offshore wind energy resources *Environ. Res. Lett.* **14** 124065
[39] Bakun A 1973 *Coastal Upwelling Indices, West Coast of North America* (US Department of Commerce, National Oceanic and Atmospheric Administration, National Marine Fisheries Service) pp 1946–71
[40] Colas F, Capet X, McWilliams J C and Shchepetkin A 2008 1997–1998 El Niño off Peru: a numerical study *Prog. Oceanogr.* **79** 138–55
[41] Jacox M G, Moore A M, Edwards C A and Fiechter J 2014 Spatially resolved upwelling in the California current system and its con-nections to climate variability *Geophys. Res. Lett.* **41** 3189–96
[42] Marchesiello P and Estrade P 2010 Upwelling limitation by onshore geostrophic flow *J. Mar. Res.* **68** 37–62
[43] Rossi V, Feng M, Pattiaratchi C, Roughan M and Waite A M 2013 On the factors influencing the development of sporadic upwelling in the Leeuwin current system *J. Geophys. Res. Oceans* **118** 3608–21
[44] Oerder V, Colas F, Echevin V, Codron F, Tam J and Belmadani A 2015 Peru-Chile upwelling dynamics under climate change *J. Geophys. Res. Oceans* **120** 1152–72
[45] Jacox M G, Edwards C A, Hazen E L and Bograd S J 2018 Coastal upwelling revisited: ekman, Bakun, and improved

upwelling indices for the U.S *West Coast. J. Geophys. Res. Oceans* **123** 7332–50
[46] Wetzel P, Haak H, Jungclaus J and Maier-Reimer E 2004 The Max-Planck-institute global ocean/sea ice model *Model MPI-OM Technical report. Retrieved From* (available at: www.mpimet.mpg.de/fileadmin/models/MPIOM/DRAFT_MPIOM_TECHNICAL_REPORT.pdf) (https://doi.org/10.1128/MCB.24.22.9942-9947.2004)
[47] Pardo P C, Padín X A, Gilcoto M, Farina-Busto L and Pérez F F 2011 Evolution of upwelling systems coupled to the long-term variability in sea surface temperature and Ekman transport *Clim. Res.* **48** 231–46
[48] He J and Mahadevan A 2021 How the source depth of coastal upwelling relates to stratification and wind *J. Geophys. Res. Oceans* **126** e2021JC017621
[49] Fox-Kemper B, Ferrari R and Hallberg R 2008 Parameterization of mixed layer eddies. Part I: theory and diagnosis *J. Phys. Oceanogr.* **38** 1145–65
[50] Capet X J, Marchesiello P and McWilliams J C 2004 Upwelling response to coastal wind profiles *Geophys. Res. Lett.* **31** 1–4
[51] Ndoye S, Capet X, Estrade P, Sow B, Machu E, Brochier T, Döring J and Brehmer P 2017 Dynamics of a "low-enrichment high-retention" upwelling center over the southern Senegal shelf *Geophys. Res. Lett.* **44** 5034–43
[52] Izquierdo A and Mikolajewicz U 2019 The role of tides in the spreading of Mediterranean outflow waters along the southwestern Iberian margin *Ocean Model.* **133** 27–43
[53] Troupin C, Mason E, Beckers J M and Sangrà P 2012 Generation of the cape ghir upwelling filament: a numerical study *Ocean Model.* **41** 1–15
[54] Casabella N, Lorenzo M N and Taboada J J 2014 Trends of the Galician upwelling in the context of climate change *J. Sea Res.* **93** 23–27
[55] Alvarez I, Lorenzo M N, DeCastro M and Gomez-Gesteira M 2017 Coastal upwelling trends under future warming scenarios from the CORDEX project along the Galician coast (NW Iberian Peninsula) *Int. J. Climatol.* **37** 3427–38
[56] Sousa M C, Alvarez I, deCastro M, Gomez-Gesteira M and Dias J M 2017b Seasonality of coastal upwelling trends under future warming scenarios along the southern limit of the Canary upwelling system *Prog. Oceanogr.* **153** 16–23
[57] Sylla A, Sanchez Gomez E, Mignot J and López-Parages J 2022 Impact of increased resolution on the representation of the Canary upwelling system in climate models *Geosci. Model Dev.* **15** 8245–67
[58] Aguirre C, Rojas M, Garreaud R D and Rahn D A 2019 Role of synoptic activity on projected changes in upwelling-favourable winds at the ocean's eastern boundaries *npj Clim. Atmos. Sci.* **2** 1–7
[59] Sylla A, Mignot J, Capet X and Gaye A T 2019 Weakening of the Senegalo–Mauritanian upwelling system under climate change *Clim. Dyn.* **53** 4447–73
[60] Miranda P M A, Alves J M R and Serra N 2013 Climate change and upwelling: response of Iberian upwelling to atmospheric forcing in a regional climate scenario *Clim. Dyn.* **40** 2813–24
[61] Soares P M, Lima D C, Cardoso R M and Semedo A 2017 High resolution projections for the western Iberian coastal low level jet in a changing climate *Clim. Dyn.* **49** 1547–66
[62] Levang S J and Schmitt R W 2020 What Causes the AMOC to Weaken in CMIP5? *J. Clim.* **33** 1535–45
[63] Stramma L 1984 Geostrophic transport in the warm water sphere of the eastern subtropical North Atlantic *J. Mar. Res.* **42** 537–58
[64] Mason E, Colas F, Molemaker J, Shchepetkin A F, Troupin C, McWilliams J C and Sangrà P 2011 Seasonal variability of the Canary current: a numerical study *J. Geophys. Res. Oceans* **116** 1–20
[65] Santana-Falcón Y, Mason E and Arístegui J 2020 Offshore transport of organic carbon by upwelling filaments in the Canary current system *Prog. Oceanogr.* **184** 102322
[66] Jing Z, Wang S, Wu L, Wang H, Zhou S, Sun B, Chen Z, Ma X, Gan B and Yang H 2023 Geostrophic flows control future changes of oceanic eastern boundary upwelling *Nat. Clim. Change* **13** 148–54
[67] Estrade P, Marchesiello P, De Verdière A C and Roy C 2008 Cross-shelf structure of coastal upwelling: a two—dimensional extension of Ekman's theory and a mechanism for inner shelf upwelling shut down *J. Mar. Res.* **66** 589–616
[68] Jacox M G and Edwards C A 2011 Effects of stratification and shelf slope on nutrient supply in coastal upwelling regions *J. Geophys. Res. Oceans* **116** 1–17
[69] Chen Z, Yan X H, Jiang Y and Jiang L 2013 Roles of shelf slope and wind on upwelling: a case study off east and west coasts of the US *Ocean Model.* **69** 136–45